# Raman Studies of Solutions of Single-Wall Carbon Nanotube Salts

**E. Anglaret,*,†,‡ F. Dragin,†,‡ A. Pénicaud,§ and R. Martel†**

*Regroupement Québécois sur les Matériaux de Pointe (RQMP) et Département de Chimie, Université de Montréal, CP 6128, Succursale Centre-ville, Montréal, Québec H3C 3J7, Canada, Laboratoire des Colloïdes, Verres, et Nanomatériaux, UMR CNRS 5587, Université Montpellier II, France, and Centre de Recherche Paul Pascal—CNRS, Université Bordeaux I, France*

*Received: August 21, 2005; In Final Form: December 14, 2005*

Polyelectrolyte solutions of Na-doped single-wall carbon nanotube (SWNT) salts are studied by Raman spectroscopy. Their Raman signature is first compared to undoped SWNT suspensions and dry alkali-doped SWNT powders, and the results indicate that the nanotube solutions consist of heavily doped (charged) SWNT. Raman signature of doping is then used to monitor in situ the oxidation reaction of the nanotube salt solutions upon exposure to air and to an acceptor molecule (benzoquinone). The results indicate a direct charge-transfer reaction from the acceptor molecule to the SWNT, leading to their gradual charge neutralization and eventual precipitation in solution. The results are consistent with a simple redox titration process occurring at the thermodynamical equilibrium.

## I. Introduction

Single-wall carbon nanotubes (SWNT) are 1D nanostructures with unique transport and optical properties. The potential use of SWNT in electronic applications stimulates research on their chemical properties and manipulation in solutions. Raw SWNT materials are often composed of nanotubes of narrowly dispersed diameters, but their chiral angle distribution is mostly random. This mixture of structures appears as a complication because their electronic properties depend directly on the diameter and chiral angle. One effective way to modify the optical and electrical responses of nanotubes is to *dope* them, i.e., to induce charge transfer from donors or acceptors. As far as alkali doping is concerned, two stable phases were observed so far in SWNT films. The so-called *saturation-doped phase* is prepared by exposing nanotubes to an excess of alkali vapors. The other is an intermediate phase observed during in situ studies of vapor phase doping. This intermediate is the so-called "phase I" associated with well-defined conductance plateaus observed in in situ conductivity experiments. The conductivity of doped mats in the saturated phase increases by about 1 order of magnitude,[1] which is directly related to the total charge transfer and concomitant with an upshift of the nanotube Fermi level.[2,3] Both phases are clearly identified by specific Raman signature. The main Raman features of the saturation-doped phase are a strong downshift and broadening of the tangential modes (TM).[4,5,6] The spectrum of "phase I" has a single TM line, broadened and slightly upshifted with respect to pristine samples.[7,8]

Phase I was recently investigated by neutron diffraction, and its structure involves alkali cations assembled around the tubes.[11] This arrangement induces a severe dilatation of the bundle lattices, which should help to promote the exfoliation of nanotube bundles in solution. Raman studies have shown a clear signature of phase I in nanotubes salts prepared by solution-based chemical reduction.[6,9] In this doping process, polyaromatic radical anions formed by alkali metal reactions are used to reduce (dope) the nanotubes with a level of charge transfer that is determined by the redox potential of the radical anions.[2,10] More recently, nanotube salts prepared by this technique have been used to dissolve nanotubes in polar aprotic solvents,[12] giving stable dispersions of nanotubes. This new technique is an alternative method to disperse nanotubes in solutions while avoiding aggressive treatments such as nanotube functionalization,[14] surfactants,[15,16] and superacids.[18] In fact, it was dubbed "dissolution douce" (soft dissolution) because it is a gentle dissolution process involving no ultrasound treatment.[13] Such true thermodynamic solutions open exciting possibilities for postprocessing of SWNT into composite fibers and films as well as controlled functionalization or redox reactions.

In this paper, we study solutions of nanotube salts (SNS) by Raman spectroscopy. Raman spectroscopy is a powerful technique for the study of the vibrational properties of both pristine[17,19] and doped carbon nanotubes.[4,5,6,7,8,9] We discuss the main features of their Raman spectra and compare them to those of aqueous supensions and alkali-doped nanotube powders. We also present a Raman study of charge neutralization processes by oxidation in air and by titration with a solution of an acceptor molecule. The materials and experimental details are presented in Section II. The Raman signatures of the SNS are presented in Section IIIA and discussed in Section IIIB. Section IIIC is devoted to the study of controlled oxidation (reverse doping) of the SNS.

## II. Experimental Section

SWNT were synthesized by the electric arc technique.[20] Their diameter lies between 1.2 and 1.5 nm, and they are generally assembled into bundles of a few tens of tubes. Nanotube salts were prepared by chemical reduction via sodium naphthalide in THF and then dissolved in DMSO as detailed elsewhere.[12] The initial concentration was 1.6 mg·g$^{-1}$ (1.4 g·l$^{-1}$), and this solution was used to prepare samples by dilution to $8 \times 10^{-2}$ mg·g$^{-1}$ ($7 \times 10^{-2}$ g·l$^{-1}$).[21] Doped samples were kept under

* Corresponding author. E-mail: eric@lcvn.univ-montp2.fr.
† Regroupement Québécois sur les Matériaux de Pointe et Département de Chimie, Université de Montréal.
‡ Laboratoire des Colloïdes, Verres, et Nanomatériaux, Université Montpellier II.
§ Centre de Recherche Paul Pascal—CNRS, Université Bordeaux I.

10.1021/jp054713l CCC: $33.50 
Published on Web 02/15/2006

inert atmosphere at all stages of the preparation. For comparison, we studied pristine powders as well as aqueous supensions prepared with sodium dodecyl sulfate (SDS) from the same nanotube samples.

The Raman experiments were carried out at three different laser energies (2.41 eV from an Ar ion laser, 1.96 eV from a He−Ne laser, and 1.17 eV from a Nd:YAG laser). The laser power was below 100 W·cm$^{-2}$ for the study of powders to avoid heating the samples. For the solutions, the laser power can be increased by more than an order of magnitude without any noticeable change in the profile of the Raman spectra, i.e. no significant heating of the samples is detected due to the much larger thermal conductivity of the liquids.

### III. Results and Discussion

**A. Raman Signatures of the Solutions.** Typical Raman spectra of the SNS samples are presented in Figure 1 and compared to those obtained from the SDS/aqueous suspensions. The use of three different laser lines is essential in our Raman studies because it helps in acquiring a better sampling. For example, the spectra in Figure 1a were measured with a laser line at 2.41 eV, which is typically the resonance energy predicted by tight-binding (TB) calculations of the third allowed optical transition (AOT) in semiconducting nanotubes with diameter of 1.2−1.5 nm.[17,19,22] Here, it is important to mention that TB alone cannot be used to calculate accurately such AOT in SWNTs because it does not treat explicitly the excited state and the excitonic interactions.[23,24] However, extended TB results, as conveniently mapped in the so-called Kataura plot, have nevertheless been successful after correction in predicting most of the enhancement effects in SWNT Raman spectra[25,26] as well as their photoluminescence peak positions.[27,28] For a single resonance model, this means that the Raman signal from SWNT of 1.2−1.5 nm diameter is largely enhanced at 2.41 eV for the semiconductor SWNTs, while excitations at 1.96 eV mostly promote the signal of the metallic tubes.

The main features in the Raman spectrum of SDS/aqueous suspensions in Figure 1 are similar to those from pristine dry samples, i.e., (i) the tangential modes (TM) display two main components assigned to circumferential (at 1565 cm$^{-1}$) and axial (at 1592 cm$^{-1}$) CC stretchings,[19] usually referred to the G$^-$ and G$^+$ bands respectively; (ii) the bunch in the range 180−200 cm$^{-1}$ is assigned to the radial breathing modes (RBM).[17,19] In contrast, the Raman spectrum is drastically different for the SNS. The signal is globally much weaker and the RBM modes are no longer present. The most significant signatures from the Raman spectra occur in the TM region, where an upshift (up to 1598−1599 cm$^{-1}$) and a significant broadening of the G$^+$ band as well as an apparent vanishing of the G$^-$ band are clearly visible. In addition, broad and intense features are observed in the ranges of 300−500 and 1300−1360 cm$^{-1}$, and a broad photoluminescence (PL) signal is superimposed onto the Raman signal. All of these features (except a weaker PL) are similar to those previously measured from alkali-doped powders.[6,7,9]

It is interesting to note that the Raman spectra in Figure 1 of the SNS excited at 1.96 eV (Figure 1b, top) and 2.41 eV are very similar, which is intriguing because the two laser lines promote different resonant Raman processes that are specific to semiconducting and metallic SWNT, respectively.[17,19,22,25,26] Moreover, the intensity drops for most of the modes, and this is especially true for the RBM. The main component of the TM upshifts from 1590 to 1598 cm$^{-1}$, and the line profile changes due to the loss of the broad and asymmetric profile of the G$^-$ band that is usually present in pristine SWNT samples. This feature was previously assigned to the Breit−Wigner−Fano (BWF) interferences in metallic nanotubes,[17,19] a profile that was found to vanish in phase I alkali-doped samples.[9] This can, therefore, be considered as a good evidence of charge-transfer doping in the SNS. Note that the relative intensity of the D-band around 1320−1350 cm$^{-1}$ is larger at 1.96 eV than that at 2.41 eV. This is also observed for pristine nanotubes. This feature is assigned to a double-resonant process that is

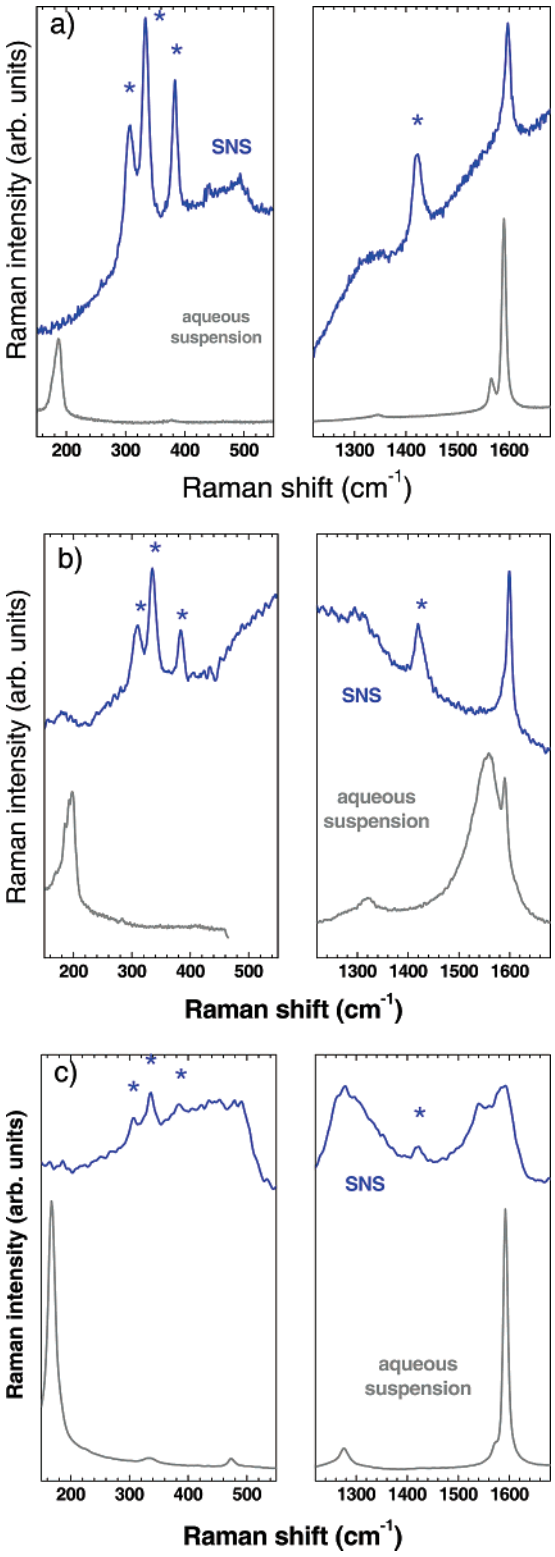


**Figure 1.** Raman spectra of solutions of nanotube salts compared to spectra of aqueous suspensions for a laser energy at (a) 2.41 eV, (b) 1.96 eV, and (c) 1.17 eV. The bands labeled with a star are from the solvent (DMSO).

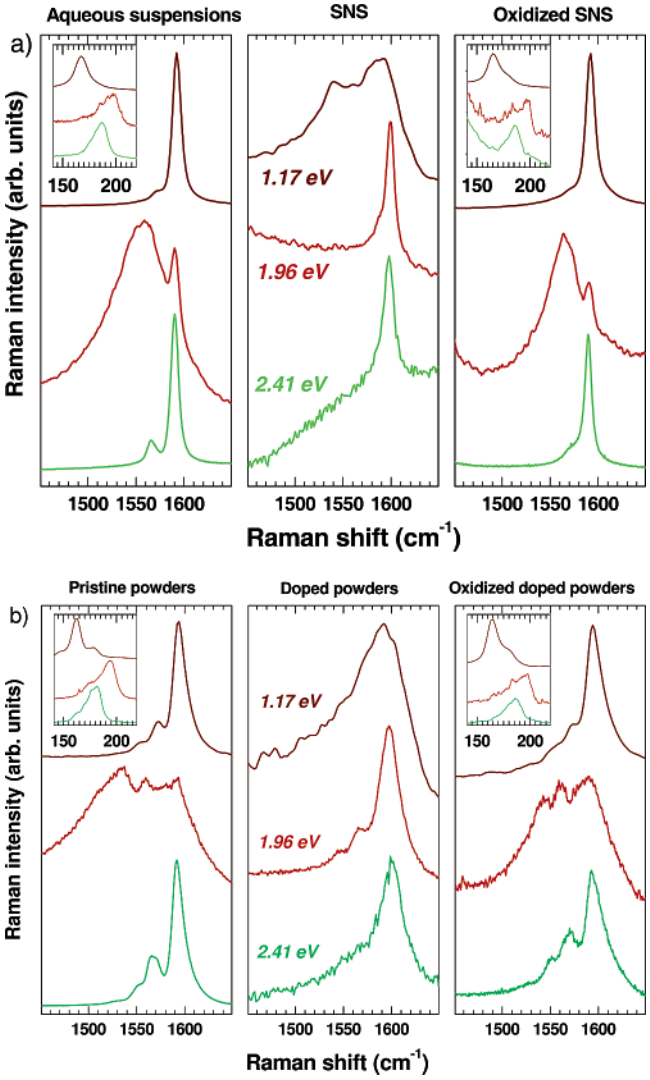


**Figure 2.** (a) Raman spectra in the TM range of aqueous suspensions, solutions of nanotube salts, and the nanotube salt solutions after oxidation in air, (b) the same from dry powders. The laser energies from bottom to top are 2.41, 1.96, and 1.17 eV, respectively. Insets: Raman spectra in the RBM range.

particularly effective for armchair nanotubes.[29] The broad feature around 480 $cm^{-1}$ is difficult to observe, and this is most likely due to the strong and broad PL signal present in our samples.

The Raman spectra of SNS excited at 1.17 eV is atypical (Figure 1c, top). This laser line corresponds typically to the energy of the second AOT of semiconducting SWNT of around 1.5 nm in diameter.[17,19,22,25,26] No upshift but a strong broadening is observed from the TM modes taken at 1.17 eV excitation. The Raman signal is abnormally large (one can compare it to that of DMSO, which can be considered as an internal reference). The signal is especially intense in the range 300−500 $cm^{-1}$ and in the range of the D-band.

A zoom on the TM spectra for doped and undoped (oxidized) solutions and powders is presented in Figure 2. This illustrates well the resemblance between the spectra taken at 2.41 and 1.96 eV for the SNS and contrasts with those taken at 1.17 eV (Figure 2a, middle). Other relevant information is the similitude between the spectra of pristine samples with the SNS taken after an oxidation in air for 48 h (Figure 2a, right).[31] The only significant difference in the TM range is the smaller intensity of the $G^-$ band for oxidized SNS. The profile of the RBM of oxidized SNS (insets in Figure 2) is also similar to that of pristine SWNT samples, but their intensity is systematically smaller with respect to that of the $G^+$ band (note in Figure 2 that the spectra are normalized for clarity). We will go further into the study of the oxidation of the SNS in the last section of the paper.

It is now interesting to compare the spectra of the solutions/suspensions with those of nanotube powders as presented in Figure 2a and b, respectively. The changes in the spectra upon doping are similar for both suspensions/solutions and the solid phase (powder). The pristine and oxidized solutions compared with the powders show a systematic but weak difference in the line width of the $G^+$ band, which is narrower, and a smaller intensity of the $G^-$ band. Note also that a slight upshift of the RBM bunch (about 5 $cm^{-1}$ at 2.41 eV, 4 $cm^{-1}$ at 1.96 eV, and 2 $cm^{-1}$ at 1.17 eV) is observed in the aqueous suspensions, as already reported elsewhere.[30] Such an upshift is systematically observed in spectra taken after air oxidation of the SNS and the doped powder samples.

*In summary, the Raman signatures of solutions of SWNT salts with diameters between 1.2 and 1.5 nm are*: (i) global drop of the Raman intensity and vanishing of the RBM for all laser energies, (ii) broadening and upshift to 1598−1599 $cm^{-1}$ of the $G^+$ band, with an apparent vanishing of the $G^-$ band, superimposed to a strong PL signal, for laser excitations at 2.41 and 1.96 eV, (iii) different signature at 1.17 eV, with a nonshifted, broad, and complex profile for the TM, (iv) broad and strong Raman signals between 300 and 500 $cm^{-1}$ and in the region of the D-band, (v) the spectra of oxidized SWNT salts in solution are very similar to the spectra from aqueous suspensions, except for a smaller intensity of the RBM and $G^-$ bands, and (vi) the spectra of solutions and powders are very similar for both doped and undoped samples, but the intensity of the $G^-$ band is smaller and the line width for the $G^+$ band is narrower for the solution samples.

We also studied solutions of nanotube salts prepared with HiPCO samples, featured by a different distribution of diameters (typically between 0.7 and 1.2 nm). Most of the Raman signatures listed above are equally observed with HiPCO samples (in particular points (i) and (iv) to (vi)), but there is at least one noticeable difference. There is no upshift of the $G^+$ band at any of the three laser excitation energies available. This was already reported for doped HiPCO powders.[32] Results from those samples will be presented elsewhere.[33]

**B. Interpretation of the Spectra.** Doping of nanotubes involves the absorption/intercalation of alkali atoms between SWNT in the bundles[11] *and* a charge transfer between the alkali atoms and the SWNT.[1,7] On one hand, the intercalation of alkali changes the structural environment and the local symmetry, and this process may induce stress on the nanotube walls. On the other hand, charge transfer is expected to modify the bond lengths between the carbon atoms[4,37] and to shift the Fermi level.[2,3] Therefore, changes in the electronic and optical properties of SWNT are expected, and those changes will directly alter the possible resonant Raman processes. We discuss below the main Raman features identified above (i to vi) with respect to doping.

*Feature (i).* The optical properties of doped SWNT are dramatically different if compared to undoped SWNT because the *i*th optical transition is no longer allowed because the final states are already occupied by the dopants. As a result, the resonant Raman process for laser excitation energies matching this optical transition is gradually turned off with doping and the Raman signal of degenerately doped SWNT should no longer be influenced by a resonance. This simple model explains well the general loss of Raman intensity upon doping seen in

our doped samples.[9] The model also explains why the spectra taken at 2.41 and 1.96 eV for doped samples are similar.

This model, however, does not explain the complete loss of the RBM mode for the SNS (Figure 1). It is likely that other factors contribute to the effect. The presence of alkali atoms near the tubes induces stress on the tubes and/or may change the local symmetry. In fact, the intensity of the RBM is known to be very sensitive to the environment. It is, for example, much weaker when tubes lie on a substrate as compared to suspended ones or when samples are exposed to hydrostatic pressure.[34,35] This suggests that the effect of the stress induced by the alkali atoms is comparable to that from the surrounding liquid. Stress may also explain the weaker intensity of the RBM for oxidized doped samples compared to pristine samples, suggesting that the alkali atoms, or their oxides, remain partially around the tubes. Indeed, alkali atom oxides have been observed on the tubes surface upon oxidation in transmission electron microscopy studies.[36]

*Feature (ii).* The width of the Raman lines is inversely proportional to the lifetime of the phonons, but the broadening of the $G^+$ band upon reduction can also be attributed to a structural disorder due to the heterogeneous decoration of the nanotube surfaces by the alkali atoms.[11] It may also be related to the loss of resonance enhancement of the Raman signal, implying here that all SWNT are contributing equally to the spectra, which adds many possibilities to TM frequencies due to the presence of different diameters, chiral angles, and/or doping levels. However, the upshift of the $G^+$ band is unexpected. The effect of *n* doping is a softening of the CC bonds for both saturation-doped graphite intercalation compounds (GIC)[37] and nanotubes,[4,5] and this should introduce a downshift of the $G^+$ band. Only for GIC at low doping levels (high doping stages), the $E_{2g2}$ mode of graphite splits and the frequency for a graphite layer bounded with an intercalant layer upshifts due to the difference of force constants arising from a change in the structural environment of the carbon atoms.[37] However, the frequency of this peak decreases with increased alkali doping, which was assigned to an expansion of the lattice in the in-plane direction.[37] By analogy with GIC, it would be tempting to assign the upshift of the TM to a new structural environment of the SWNT salts, i.e. to carbon−alkali interactions. However, the same upshift of the TM should be observed after oxidation in air, at least for the powders, which is not seen in our experiment (Figure 2b, right). Furthermore, one would expect an upshift also for HiPCO samples, which is not actually observed in the experiments.[33] All of this indicates that the upshift of the TM in the SNS is more complex and does not come from structural changes. Moreover, it is unlikely that *n* doping induces an important dilatation of the CC bond. Therefore, the interpretation of the TM upshift remains an open question and calculations will be necessary to help understanding these electronic changes in the doped samples. Here, the possibility of double-resonance processes may provide a plausible explanation.[38]

By contrast, the apparent vanishing of the $G^-$ band in SNS samples (Figure 2) can be well understood. The $G^-$ band is assigned to carbon−carbon stretch along the circumference of the tube, and this band is, therefore, expected to be more sensitive to the structural environment than the axial $G^+$ band. Moreover, a drop of the $G^-$ band intensity is observed in aqueous suspensions with respect to powders (Figure 2a and b, left), and the intensity of the $G^-$ band remains weak after the oxidation of the SNS in air. Therefore, we interpret the drop of the $G^-$ band by the absorption/intercalation of alkali atoms around the nanotubes. The broad and asymmetric profile of the $G^-$ band for pristine samples is assigned to Breit−Wigner−Fano (BWF) interferences between phonons and plasmons in metallic tubes.[39] Such interferences are observed in bundles in pristine nanotube samples, but it is not present in individual nanotubes[40,41] because of different plasmon properties of isolated nanotubes.[42] The loss of the BWF profile in the SNS is yet an additional evidence of the changes in the electronic properties of the SWNT by alkali doping. The much narrower profile of the $G^-$ band of oxidized SNS samples at 1.96 eV suggests that some alkali atoms are still decorating the nanotubes after the oxidation step. It can also result from the exfoliation of the bundles during the salt formation. In fact, a clear Raman signature of exfoliation, if it exists, is yet unknown to us. Finally, the origin of the strong PL signal from our samples is not clear at the moment; it may arise from impurities or defects in the samples. It may alternatively be an intrinsic property of the solubilized tubes.

*Feature (iii).* The TM spectra of doped samples from both powders and solutions are clearly different when the Raman spectrum is excited at 1.17 eV (Figure 2a and b, middle). Therefore, the simple model involving the "loss of the resonance" fails to interpret the whole data set. It is tempting to correlate these atypical spectra to a new resonance coming from an absorption band located near 1.2 eV, as previously seen in spectra of Li-doped nanotube films[10] and in K-doped nanotube powders[43] (not shown). Thus, the larger Raman intensity and the atypical profile of the TM for 1.17 eV excitation must probably involve a new resonant effect whose origin remains unclear.

*Feature (iv).* We now discuss the modes in the ranges 300−500 and 1300−1360 $cm^{-1}$ (D-band region). New modes were observed for saturation-doped materials at low frequencies[5] and in the range 900−1400 $cm^{-1}$.[4,5] The frequency of the low-frequency modes were found to depend on the nature of the alkali atoms and they were, therefore, assigned to new vibrations involving the alkali atoms.[5] Here, these modes are upshifted with respect to those for Cs or Rb, which supports such an assignment. The other modes at higher frequencies in materials doped to saturation were assigned to modes involving only the carbon atoms, modes that are inactive in pristine samples but activated in doped samples by the changes of symmetry and selection rules.[4,5] For the SNS samples, the frequency of those modes resembles those of the D-band of pristine samples (Figure 1). This D-band corresponds to the Raman signature of LO phonons near the K-point, activated by a double-resonance process.[29] Such a double-resonance process is still possible for doped samples. The broadening of the peak may, therefore, be due to changes in the band structure. However, its intensity is known to be very sensitive to the amount of defects and, more generally, to symmetry breaking. Thus, the intercalation of alkali atoms nearby the nanotubes may, by itself, explain the increase of intensity of the D-band.

*Feature (v).* The similarities between the spectra from pristine SWNT and oxidized SNS samples show that charge transfer is responsible for the main changes (TM upshift and global drop of intensity) in the Raman. These changes are reversible. However, as discussed above, we assign the incomplete reversibility of some of the features (loss of intensity of the RBM and $G^-$ band) to permanent changes in the structural environment of the SNS samples due to the intercalation of alkali ions.

*Feature (vi).* The similarities between the Raman spectra from doped powders and SNS confirm that the solubilized nanotubes are negatively charged. Interactions with solvent molecules have

only a small effect on the intensity and frequency of the RBM and $G^-$ bands. The broader line width of the TM in oxidized doped powders is assigned to some structural heterogeneities and/or to shorter phonon lifetimes.

**C. Control of the Charge Density by a Redox Titration Process.** One of the key features of the solutions with respect to powders is the possible control of their properties by selective chemical reactions in solution. Here, we illustrate how the charge density can be controlled by a simple redox titration process. This also allows us to confirm a posteriori the interpretation of the Raman signatures of the SNS. The solutions of nanotube salts were titrated with a solution of benzoquinone in DMSO. Benzoquinone was selected because its radical anion forms with a redox potential of −0.4 V, which is of the same order of magnitude as that for SWNT of 1.2−1.5 nm in diameter.[10,44] During the titration, one can observe the formation of nanotube aggregates, assigned to undoped, and consequently unsoluble, nanotubes. A given titration volume does not undope all the nanotubes because the energy of the van Hove singularities and possibly the redox potential vary as a function of diameter and chiral angle. After each titration step, the samples are centrifuged in order to form a deposit with the aggregates. Figure 3 displays the evolution of the Raman spectra of the supernatant in the TM range for different titration volumes. Spectra at 2.41 eV (Figure 3a) show a $G^+$ band that is progressively narrower and downshifted. The $G^-$ band, around 1565 $cm^{-1}$, is not visible during the early stage of the reaction, but it appears in the last stages, i.e., when the spectrum of an undoped suspension is almost completely recovered. Note that the intensity of the TM increases during the early stages, goes through a maximum that is assigned to resonance effects, and then drops because of the decreasing concentration in the supernatants (not visible in the normalized spectra of Figure 3). The detailed interpretation of the changes in the Raman intensity during the titration process falls out of the scope of this paper and will be discussed elsewhere.[33]

The gradual evolution of the Raman spectra from SNS during oxidation is also observed with Raman taken at 1.96 eV (Figure 3b). The BWF profile of the $G^-$ band is also recovered at the final stages of oxidation (Figure 3b, top), and the continuous and progressive changes in the spectra are assigned to electron transfer from the SWNT to the benzoquinone. As discussed above, the frequency and profile of the TM can be directly related to the charge density on the SWNT, and this is true at any stage of oxidation. To illustrate this, we fitted the spectra taken at 2.41 eV with a sum of two Lorentzians, assigned to the $G^-$ and $G^+$ bands. Good fits were achieved for all spectra, but the error bars on the Lorentzian parameters for the $G^-$ band were large because of the rather poor signal-to-noise ratio of the data. Figure 4 displays the frequency and line width of the $G^+$ band. Note that a downshift of a few $cm^{-1}$ is observed when the initial solution (open symbol on Figure 4) is diluted. This is likely coming from a partial oxidation due to the presence of residual water or oxygen in DMSO. In the last steps of the titration, the $G^+$ band reaches the 1592 $cm^{-1}$ value, which is typical for pristine SWNT. A minimum is also observed when most, if not all, charges have been transferred ($R = 1-3$ in Figure 3). The amplitude of this shallow minimum is close to the resolution of the experiment. Trying to explain this minimum raises an important question: how can there be nanotubes in the supernatant when the oxidation−titration reaction is complete? They are supposed to precipitate because undoped SWNT is insoluble in DMSO. First, it may take a longer time to precipitate them because of a slow kinetic process, or a small

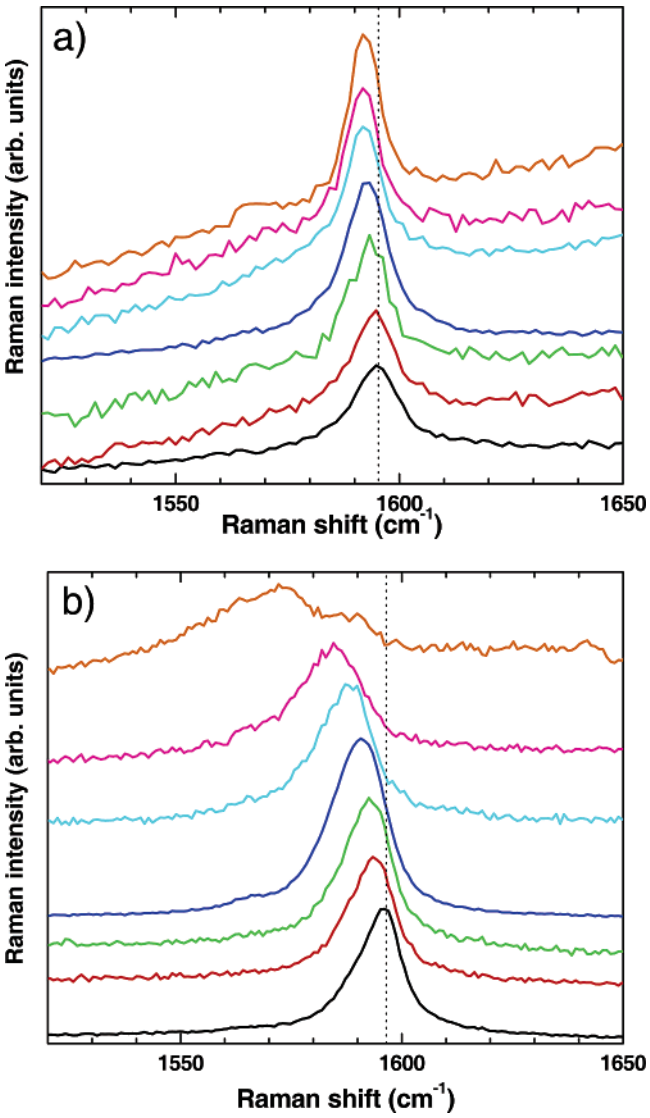


**Figure 3.** Evolution of the TM spectrum in the supernatant of a solution titrated with various quantities of benzoquinone in DMSO. From bottom to top, the molar ratio of benzoquinone and alkali atoms are 0, 0.07, 0.15, 0.31, 0.79, 1.46, and 23.22, respectively. The spectra are taken with laser energy of (a) 2.41 eV and (b) 1.96 eV. The intensities were normalized for clarity (see text).

amount of undoped nanotubes may be stable in the supernatant due to unknown reasons. On the other hand, the difference in the redox potential of benzoquinone and some nanotubes can be large enough so that a complete oxidation of all the SWNT is impossible. Last, it could be higher, inducing a reverse doping of some SWNT with positive charges. Further experiments with other titrants will be necessary in order to understand this last point.

Finally, we discuss the evolution of the line width of the $G^+$ band (inset in Figure 4). It gets continuously narrower during the titration process. The final value (8 $cm^{-1}$ for full width at half-maximum) is close to that of undoped nanotubes in aqueous suspensions. This result does not support the hypothesis of a disorder-induced broadening in the SNS. Therefore, we assign the broadening of the TM in the SNS to the sum of the contributions coming from nonresonant nanotubes having various diameters, chiral angles, and/or doping levels.

## IV. Conclusion

The Raman signatures of solutions of nanotube salts were identified and discussed. The spectra are very similar to those

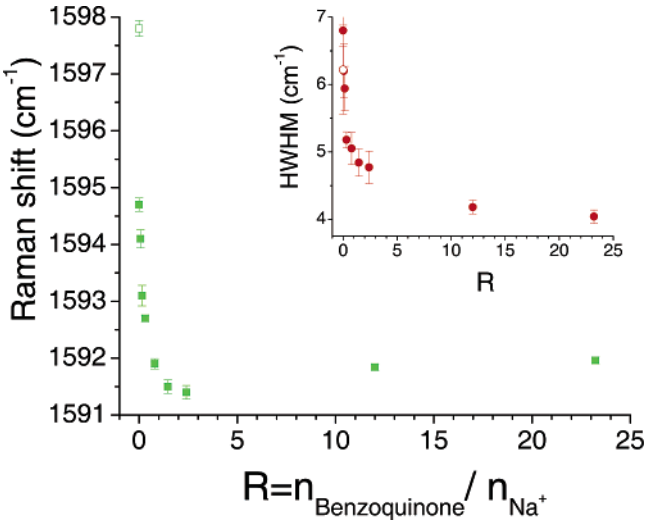


**Figure 4.** Frequency and line width (inset: half width at half-maximum) of the $G^+$ band for the solution reacted with various quantities of benzoquinone. The open symbol is for the initial solution, i.e., before dilution (see text).

of alkali-doped dry powders. The main features are the loss of the resonance (photoselection) process, leading to a general loss of intensity and the disappearance of the radial breathing modes as well as a broadening and an upshift of the tangential modes. Several features remain unexplained. Calculations of the band structure and vibrational properties of doped SWNT would be helpful to interpret completely the spectra. In particular, a clear understanding of the influence of charge transfer on the softening or hardening of Raman modes could be of invaluable help in the growing fields of redox chemistry of nanotubes[44] or nanotube-based actuators.[45] Finally, it was shown that charge density on the nanotubes can be controlled by a simple oxidative titration process. This preliminary information demonstrates the interest of such solutions of nanotube salts in order to modify and control the electronic properties of SWNT by chemical reactions.

**Acknowledgment.** We acknowledge fruitful discussions with Nedjma Bendiab, Matthieu Paillet, Stéphane Auvray, Jean-Louis Sauvajol, and Pierre Petit. The Montreal group thanks Antonella Badia and Nathalie Ravet for welcoming us in their labs. This work was in part funded by the Université de Montréal, the RQMP, and the Canada Research Chair program. It was also carried out in the framework of the GDRE CNRS no. 2756 "Science and applications of the nanotubes NANO-E" and a Fond France−Canada program. A.P. and E.A. acknowledge the Consulat Général de France à Québec for financial support. E.A. acknowledges the DGA for financial support. A.P. acknowledges the Ministère des Relations Internationales du Québec for financial support.

## References and Notes

(1) Lee, R. S.; Kim, H. J.; Fischer, J. E.; Thess, A.; Smalley R. E. *Nature* **1997**, *388*, 255.
(2) Jouguelet, E.; Mathis, C.; Petit, P. *Chem. Phys. Lett.* **2000**, *318*, 561.
(3) Jo, C.; Kim, C.; Lee, Y. H. *Phys. Rev. B* **2002**, *65*, 035420.
(4) Rao, A. M.; Eklund, P. C.; Bandow, S.; Thess, A.; Smalley, R. E. *Nature* **1997**, *388*, 257.
(5) Bendiab, N.; Righi, A.; Anglaret, E.; Sauvajol, J. L.; Duclaux, L.; Béguin, F. *Chem. Phys. Lett.* **2001**, *339*, 305.
(6) Sauvajol, J. L.; Bendiab, N.; Anglaret, E.; Petit, P. *C. R. Phys.* **2003**, *4*, 1035.
(7) Bendiab, N.; Spina, L.; Zahab, A.; Poncharal, P.; Marlière, C.; Bantignies, J. L.; Anglaret, E.; Sauvajol, J. L. *Phys. Rev. B* **2001**, *65*, 153407.
(8) Chen, G.; Furtado, C. A.; Bandow, S.; Iijima, S.; Eklund, P. C. *Phys. Rev. B* **2005**, *71*, 045408.
(9) Bendiab, N.; Anglaret, E.; Bantignies, J. L.; Zahab, A.; Sauvajol, J. L.; Petit, P.; Mathis, C.; Lefrant, S. *Phys. Rev. B* **2001**, *64*, 245424.
(10) Petit, P.; Mathis, C.; Journet, C.; Bernier, P. *Chem. Phys. Lett.* **1999**, *305*, 370.
(11) Cambedouzou, J.; Rols, S.; Bendiab, N.; Almairac, R.; Sauvajol, J. L.; Petit, P.; Mathis, C.; Mirebeau, I.; Johnson, M. *Phys. Rev. B*, **2005**, *72*, 041404.
(12) Pénicaud, A.; Poulin, P.; Derré, A.; Anglaret, E.; Petit, P. *J. Am. Chem. Soc.* **2005**, *127*, 8.
(13) Pénicaud, A.; Poulin, P.; Anglaret, E.; Petit, P.; Roubeau, O.; Enouz, S.; Loiseau, A. *Electron. Prop. Novel Mater.—Proc. Int. Workshop*, **2005**, in press.
(14) Tasis, D.; Tagmatarchis, N.; Georgakilas, V.; Prato, M. *Chem.—Eur. J* **2003**, *9*, 4000.
(15) Vigolo, B.; Pénicaud, A.; Coulon, C.; Sauder, C.; Pailler, R.; Journet, C.; Bernier, P.; Poulin, P. *Science* **2000**, *290* 1331.
(16) Wenseleeres, W.; Vlasov, I. I.; Goovaerts, E.; Obratsowa, E. D.; Lobach, A. S.; Bouwen, A. *Adv. Funct. Mater.* **2004**, *14*, 1105.
(17) Sauvajol, J. L.; Anglaret, E.; Rols, S.; Alvarez, E. *Carbon* **2002**, *40*, 1789.
(18) Ramesh, S.; Ericson, L. M.; Davis, V. A.; Saini, R. K.; Kittrell, C.; Pasquali, M.; Billups, W. E.; Adams, W. W.; Hauge, R. H.; Smalley, R. E. *J. Phys. Chem. B* **2004**, *108*, 8794.
(19) Dresselhaus, M. S.; Dresselhaus, G.; Saito, R.; Jorio, A. *Phys. Rep.* **2005**, *409*, 47.
(20) Journet, C.; Maser, W. K.; Bernier, P.; Loiseau, A.; de la Chapelle, M.; Lefrant, S.; Deniard, P.; Lee, R.; Fischer, J. E. *Nature* **1997**, *388*, 756.
(21) Note that these concentrations only indicate: (i) these are concentrations in salts, of formula $Na(THF)C_{10}$, hence the concentrations in nanotubes are lower by a factor 120/215 = 0.56; (ii) the formula unit was obtained by chemical analysis and thus integrates carbon impurities that are common in electric arc samples.
(22) Kataura, H.; Mumazawa, Y.; Maniwa Y.; Umezu, I.; Suzuki, S., Ohtsuka, Y., Achiba, Y. *Synth. Met.* **1999**, *103*, 2555.
(23) Wang, F.; Dukovic, G.; Brus, L. E.; Heinz, T. F. *Science* **2005**, *308*, 838.
(24) Maultzsch, J.; Pomraenke, R.; Reich, S.; Chang, E.; Prezzi, D.; Ruini, A.; Molinari, E.; Strano, M. S.; Thomsen, C.; Lienau, C. *Phys. Rev. Lett.*, **2006**, in press.
(25) Fantini, C.; Jorio, A.; Strano, M. S.; Dresselhaus, M. S.; Pimenta, M. A. *Phys. Rev. Lett.* **2004**, *193*, 147406.
(26) Jorio, A.; Fantini, C.; Pimenta, M. A.; Capaz, R. B.; Samsonidze, G. G.; Dresselhaus, G.; Dresselhaus, M. S.; Jiang J.; Kobayashi, N.; Gruneis, A.; Saito, R. *Phys. Rev. B* **2005**, *71*, 075401.
(27) Bachilo, S. M.; Strano, M. S.; Kittrell, C.; Hauge, R. H.; Weisman, R. B.; Smalley, R. E. *Science* **2002**, *298*, 2361.
(28) Hagan, A.; Hertel, T. *Nano Lett.* **2003**, *3*, 383.
(29) Maultzsch, J.; Reich, S.; Thomsen, C. *Phys. Rev. B* **2001**, *64*, 121407.
(30) Izard, N.; Riehl, D.; Anglaret, E. *Phys. Rev. B* **2005**, *71*, 195417, 2005.
(31) Note that for these oxidized samples, the word "solution" is not relevant anymore because formation of aggregates and flocculation are observed when the samples are exposed to air. The spectra in Figure 2 were measured by agitating the oxidized samples to homogenize them, but the spectra were actually very similar when the laser beam was focused on the aggregates sedimented at the bottom of the cells.
(32) Kukovecz, A.; Pichler, T.; Pfeiffer, R.; Kramberger, C.; Kuzmany, H. *Phys. Chem. Chem. Phys.* **2003**, *5*, 582.
(33) Dragin, F. et al. to be published.
(34) Lu, J.; Nagase, S.; Zhang, S.; Peng, L. *Phys. Rev. B* **2004**, *69*, 205304.
(35) Venkateswaran, U. D.; Rao, A. M.; Richter, E.; Menon, M.; Rinzler, A.; Smalley, R. E.; Eklund, P. C. *Phys. Rev. B* **1999**, *59*, 10928.
(36) Enouz, S.; Loiseau, A.; Pénicaud, A. Private communication.
(37) Dresselhaus, M. S.; Dresselhaus, G. *Adv. Phys.* **1981**, *30*, 139.
(38) Maultzsch, J.; Reich, S.; Thomsen, C. *Phys. Rev. B* **2002**, *65*, 233402.
(39) Brown, S. D. M.; Jorio, A.; Corio, P.; Dresselhaus, M. S.; Dresselhaus, G.; Saito, R.; Kneipp, K. *Phys. Rev. B* **2001**, *63*, 155414.
(40) Bendiab N.; Almairac, R.; Paillet, M.; Sauvajol, J. L. *Chem. Phys. Lett.* **2003**, *372*, 210.
(41) Paillet, M.; Poncharal, P.; Zahab, A.; Sauvajol, J. L.; Meyer, J. C.; Roth, S. *Phys. Rev. Lett.* **2006**, in press.
(42) Kempa, K. *Phys. Rev. B* **2002**, *66*, 195406.
(43) Petit, P. Private communication.
(44) O'Connell, M. J.; Eibergen, E. E.; Doorn, S. K. *Nat. Mater.* **2005**, *4*, 412.
(45) Gupta, S.; Hughes, M.; Windle, A. H. *J. Appl. Phys.* **2004**, *95*, 2038.